buildings

Article

Shear Behavior of Prestressed Hollow Core One-Way Slabs with Openings: Experimental, Numerical, and Standard Formulation Verification

Gregory Pinheiro [1], Armando Moreno Júnior [2], Arturo Schultz [3], Igor Silva [1], Felipe N. Arroyo [1,*], Vinícius Aquino [4], Marcelo Ferreira [1], Roberto Carvalho [1], Herisson Santos [5], André L. Christoforo [1] and Fernando Almeida Filho [1]

[1] Department of Civil Engineering, Federal University of São Carlos, Washington Luís Highway, km 235, São Carlos 13565-905, Brazil; gregoryleepinheiro@gmail.com (G.P.); igor.pacchioni@unasp.edu.br (I.S.); marcelof@ufscar.br (M.F.); robertochustcarvalho@gmail.com (R.C.); christoforoal@yahoo.com.br (A.L.C.); almeidafilho@ufscar.br (F.A.F.)
[2] Structures Department, University of Campinas, Avenue Albert Einstein 951, Campinas 13083-970, Brazil; almoreno@fec.unicamp.br
[3] Department of Civil, Environmental, and Geo-Engineering, University of Minnesota, 500 Pillsbury Drive SE, Minneapolis, MN 55455, USA; aeschultz@umn.edu
[4] Department of Civil Engineering, Federal University of the South and Southeast of Pará, St. Geraldo Ramalho, 33, Santana do Araguaia 68560-000, Brazil; aquino.vini@hotmail.com
[5] Federal Institute of Education Science and Technology of Rondônia, Vilhena 76870-000, Brazil; herisson.santos@ifro.edu.br
* Correspondence: lipe.arroyo@gmail.com; Tel.: +55-(17)-992842500

Abstract: The use of prestressed precast hollow core slabs has intensified as technological advances. However, the knowledge of the structural behavior when openings are inserted into this element is still limited, mainly due to the shear force. Therefore, the present study aims to analyze the structural behavior of the shear test of prestressed hollow core slabs with openings. In this paper, three types of hollow core slabs were tested: no openings, a central opening and side openings; using experimental and numerical methodology. The experimental test was carried out in the Federal University of São Carlos, and the numerical analysis used the software ABAQUS. All results were compared with three standard formulations (i.e., NBR, ACI and Eurocode), in order to verify its accuracy. In the end, the numerical results demonstrated that the developed model (CDP) presented results close to the experimental results. For the hollow core slab with a central opening, a rupture occurred in the web adjacent to the opening. On the other hand, for the hollow core slab with side openings, the rupture occurred at the edge of the web. Therefore, it was possible to conclude that the openings influence the main web tensions, being responsible for the diagonal model stress rupture. Finally, the Brazilian and Eurocode standard formulations proved to be good estimators of the resistant shear force.

Keywords: precast concrete; prestressing; finite element method; structural behavior; shear force

check for updates

Citation: Pinheiro, G.; Moreno Júnior, A.; Schultz, A.; Silva, I.; Arroyo, F.N.; Aquino, V.; Ferreira, M.; Carvalho, R.; Santos, H.; Christoforo, A.L.; et al. Shear Behavior of Prestressed Hollow Core One-Way Slabs with Openings: Experimental, Numerical, and Standard Formulation Verification. *Buildings* **2023**, *13*, 1857. https://doi.org/10.3390/buildings13071857

Academic Editor: Ahmed Senouci

Received: 26 June 2023
Revised: 14 July 2023
Accepted: 19 July 2023
Published: 22 July 2023

1. Introduction

An economic and popular solution for flooring in buildings, hollow core (HC) slabs are prefabricated floor slabs widely used around the world, being used on commercial, industrial and parking buildings [1–3]. In buildings, hollow core slabs demand openings to accommodate mechanical and plumbing installations (i.e., shafts). However, structural openings, which impose the cut of strands, cause modifications on the load distribution along all slabs, creating a weak point in the structure [1,3,4].

For the correct structural design of hollow core slabs, there are American [5], European [6] and Brazilian [7,8] standards. In order to adhere to adequate structural demands with the presence of openings, hollow core designs already consider the structural openings and the industry rearranges the distribution of strands, adding strands along the remaining cross-section. However, during the lifespan of the hollow core slabs, sometimes it is necessary to create an opening not planned by a responsible engineer [2–4,9].

These openings mainly affect the shear strength of the hollow core slab, when compared to flexural strength. In the literature, there is research considering the design of hollow core slabs under shear loading [10,11], evaluating the analysis of HC slabs reinforced with fibers [2,4,9,12]. However, these pieces of research use the bending test for such evaluation, not a shear test, as prescribed by the FIP [13]. Also, there is a behavior analysis of the HC slab with an opening at the slab edge, reinforced with polymer fiber [2].

Considering the different conditions that each building requires to fit the HC plates, it is important to evaluate the opening at different positions on the edge of the prestressed HC plates. Likewise, it is necessary to evaluate the behavior of the concrete and wires throughout the load tests for a better understanding of the performance. Therefore, a numerical methodology becomes an alternative since it is possible to better analyze the stress distribution in the slab section.

Alternatively, normative standards (ACI 318 [5], Eurocode 2 [14] and ABNT NBR 14861 [8]) can be used to predict the resistant shear force. However, these standards in the world do not prescribe to or define the proceedings to be taken considering the openings; they consider their effects on load and distribution along the member, highlighting the importance of the present research for a better understanding for designers. In normative standards across the world, different methods are presented to calculate design-resistant shear force on prestressed members, as presented in normative formulations later.

In view of this, since the norms do not consider openings in their formulation, this paper aims to contribute to the study of openings on prestressed hollow core slabs. The present research proposed to analyze the behavior of HC slabs with openings on the edge subjected to shear force and compared the experimental results with the normative formulations, aiming to analyze their accuracy. In addition, numerical simulations in Abaqus software (version 2017) were developed, in order to calibrate the CDP model for this type of structure, since it is widely used only in simulations of reinforced concrete structures. Moreover, through the numerical simulations, it was possible to analyze the behavior of stress distribution and material rupture. Finally, the experimental and numerical values are compared with those obtained by the standard [5,8,14], thus verifying the quality of its equations for estimating the resistant shear force.

2. Materials and Methods

2.1. Materials Characterization

Five specimens (dimensions of 200 mm × 1245 mm × 6000 mm) of industrial prestressed hollow core slabs were tested to analyze the effect of openings on a prestressed hollow core. For the slab production, concrete was used with 35 MPa of theoretical strength (fck), produced by Rotesma® Precast Concrete Company im Brazil (Chapecó, Brazil). The concrete was composed of Portland cement CPV ARI [15], with 19 mm nominal coarse aggregates, chemical additives and mineral additions to improve the concrete mix, produced on concrete central with automatized dosage. The concrete mix was not provided by the company by industrial secrecy. The unit weight of concrete was close to 2400 kg/m^3. The slab was fabricated with 8 strands composed of 7 wires with low relaxation (9.5 mm diameter each). The ultimate tensile strength of 1900 MPa, elasticity modulus of 200 GPa and nominal area of 56 mm^2 was used. Strands were placed on the slab with a force of 83.2 kN on each strand.

In order to obtain a reference of compressive and tensile strengths and elasticity modulus of the concrete, cylindrical concrete specimens 100 × 200 mm were molded, cured and tested following the disposal of Brazilian Standards ABNT NBR 5738 [16] and NBR 5739 [17]. These norms recommend that the test be performed at 28 days, but the hollow core slabs were tested at 59 days, requiring the correction of this value to 28 days (according to the Brazilian normative, the force was reduced by 20% for this correction). The results are shown in Table 1.

Table 1. Concrete characterization tests results.

Test	Test Day (59 Days)	Converted to 28 Days
Compressive Strength (MPa)	48.41	39.09
Tensile Strength (MPa)	3.68	2.94
Elasticity Modulus tangent (GPa)	34.97	30.62

For the strands used in the slab production, the characterization report given by the manufacturer was utilized [18].

2.2. Testing Procedure

The variables in this paper were the openings on the slabs. In this study, two types of openings were studied: side and central. In all, 5 hollow core slabs were tested, one reference slab (without opening), two with central openings and two with side openings (Table 2). It is worth mentioning that the dimensions were the same for all slabs (200 mm × 1245 mm × 6000 mm), and the opening is 400 mm × 400 mm. The openings were defined randomly, being justified by a necessary size to allow the passage of water and electrical pipes. It should also be noted that the openings were made in the normal part, i.e., the slab was not concreted with the opening. The specimens were cut later for the required opening size.

Table 2. Specimens used in the research and their identifications.

Specimen Name	HC Sketch	Kind of Test	Identification
Reference		Shear strength	HCS-01
Side opening	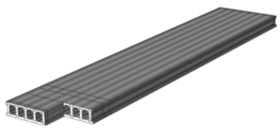	Shear strength	HCC-02
Central opening		Shear strength	HCL-03

For the test instrumentation, the equipment used was a hydraulic press with 500 kN of capacity with an electric pump and manual controller, load cell with 600 kN of capacity, reaction gantries with 2000 kN capacity, Linear Variable Differential Transformers (LVDT) and data acquisition system. The proposed program used the same test setup as the one exposed on the European code EN 1168 [19] and suggested by the FIP [13] for determining the slab shear strength capacity, as shown in Figure 1.

The loading was applied at the distance from the roller support of 2.5·h (Figure 2a), being "h" the thickness. Moreover, was introduced a steel stiff transverse beam, with the depth of 250 mm and stiffness sufficient to prevent an unequal distribution of the load over its width (Figure 2b). The interface between the element and the support beam, an elastomeric plate with 10 mm of thickness was used. This material compensated for the element surface unevenness and the supports were able to distribute uniformly the reactions preventing located loads or torsion [20]. It is worth mentioning that the tests were performed at a temperature of 37 °C.

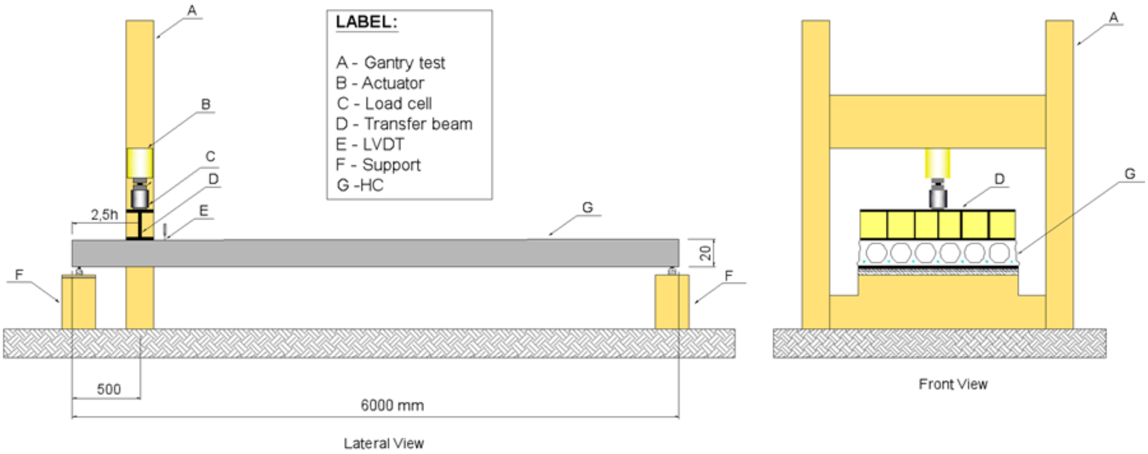

Figure 1. Shear strength test setup.

(**a**) (**b**)

Figure 2. Positioning of the slabs (**a**) and load transferring steel beam positioning (**b**).

In all tests, the force × displacement curve was extracted. The displacement was obtained through two LVDTs (i.e., one on the right side and one on the left side). The LVDTs position is shown in Figure 1 (label E), being the final displacement determined by the average of the two measured displacements. The strands were positioned and numbered following the disposed below (Figure 3).

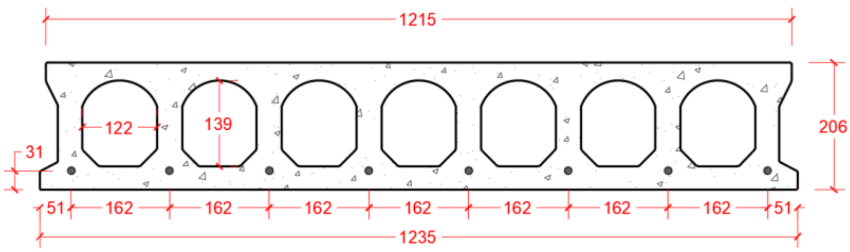

Figure 3. Positioning of the strands and their respective numbering.

For the analysis of strand slipping, Brazilian Standard ABNT NBR 14861 [8] establishes the following equation for strand slip mean value, presented on Equation (1).

$$\Delta l_0 = 0.40 \cdot l_{pt2} \cdot \frac{\sigma_{cp0}}{E_p} \tag{1}$$

With Δl_0 being the strand slip, σ_{cp0} the prestressing tension at the moment of prestress release, E_p the reinforcement modulus of elasticity and l_{pt2} the higher design value for the transmission length (set at 85ϕ, with ϕ the strand diameter). It is worth noting that the maximum strand slip must not be higher than 30% of the mean value calculated [8].

2.3. Numerical Analysis

In addition to the reference model without opening (HCS-01), the model with a central opening (HCC-02) and side opening (HCL-03) was also simulated. The numerical models have been previously described in Table 3.

Table 3. Parameters for the stress × strain curve equations.

Strength Class	Cement Class	α_a	α_d	ε_p (10^{-3})
C20, C30	32.50	2.20	0.40	1.40
	42.50	1.70	0.80	1.60
C40	42.50	1.70	2.00	1.80

2.3.1. Discretization of Elements

To reproduce the geometry and components of the structure investigated experimentally, the hollow core slabs, prestressing cables, beams (i.e., support for the slab during the test) and the metal beam (i.e., to distribute the concentrated load application) were modeled (Figure 4). The slab was modeled with the solid-type element C3D8R, the prestressing cables with the T3D2 truss bar element, and the support beams as the load application, and also the solid element discretized as rigid. As an example, the following figure shows the numerical model for the HCS-01 case (without openings).

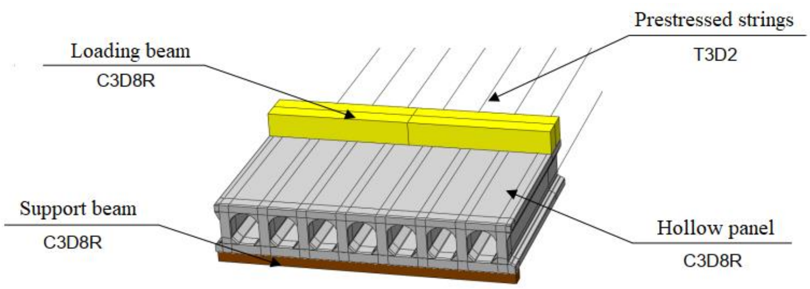

Figure 4. Numeric model HCS-01.

To reduce the computational time, as indicated by Nguyen, Tan and Kanda [21], a mesh with an opening of 100 mm was used along the longitudinal part section (Figure 5a). In the cross-section, a 10 mm mesh opening was applied in order to avoid unstructured meshes (Figure 5b). Although, in regions with large geometric irregularities, meshes were generated by sweeping. However, it is worth mentioning that a mesh test was performed.

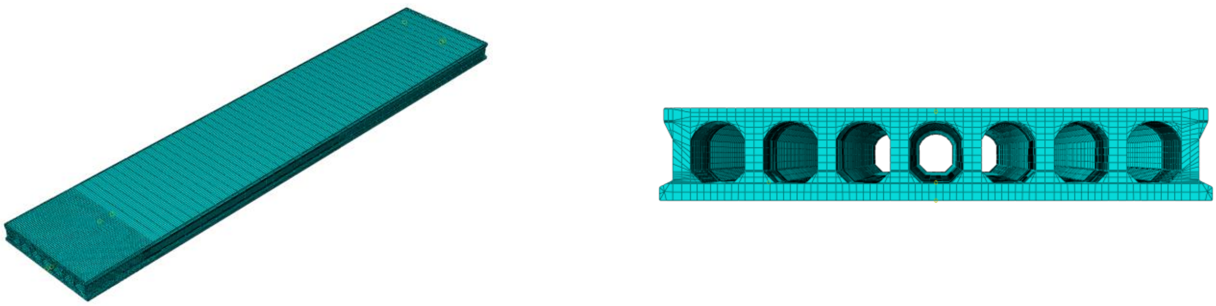

(**a**) (**b**)

Figure 5. Mesh used in the numerical simulation: (**a**) longitudinal and (**b**) in the cross-section.

2.3.2. Constitutive Model of Materials

The steel material behavior, used for the active reinforcement of the hollow core slab, was idealized by the behavior presented by NBR 6118 [7]. In addition to these properties, the density used was 7.85×10^{-6} Kg/mm^3, an elastic modulus used was 199,346.667 N/mm^2 and a Poisson's ratio of 0.30 was used.

For concrete and in order to simulate the non-linear response, the CDP (Concrete Damage Plasticity) model was adopted. This model developed by Lubliner et al. [22] and Lee and Fenves [23] is able to predict the behavior of fragile materials characterized by damaged plasticity, where it uses the tensile damage curve (tensile stress x strain), cracks, compression and crushing. Thus, parameters for the stress and strain curve equations were defined, as shown in Table 3 and indicated by Guo [24]. Since the concrete used in the research has a compressive strength of 35 MPa, an interpolation of these values was made.

The concrete strength values, as already informed in Table 1, were extracted from laboratory results, with 2.94 MPa for tensile stress, 39.09 MPa for compression, an elastic modulus of 30,620 MPa and a compression strain of 3‰. In addition to these concrete properties, it is necessary to enter the expansion angle (ψ), which is the internal friction angle of the concrete (28°); the eccentricity (*E*), calculated as a ratio of the tensile strength to the compressive strength, with a value of 0.10; the parameter f_b0⁄f_c0, being the ratio of the force in the biaxial state to the force in the uniaxial state, worth 1.16; the parameter Kc, recommended by ABAQUS as 0.667; and lastly the viscosity (υ), also recommended by ABAQUS as 0.0005. The density and Poisson's ratio of the concrete were 2.5×10^{-6} Kg/mm^3 and 0.20, respectively.

Finally, in addition to the parameters and coefficients presented, it is still necessary to insert the concrete tensile and compression damage (Table 4). In this way, to the extent that a certain inelastic deformation was reached, there was a certain damage for that respective deformation, i.e., the model goes through a cracking process, with the insertion of material nonlinearities at each new step. This damage is also reported by Guo [24].

Table 4. Concrete damage.

Compression Damage		Tensile Damage	
Inelastic Deformation (‰)	**Damage (%)**	**Inelastic Deformation (‰)**	**Damage (%)**
0.0000	0.0000	0.0000	0.0000
0.8793	0.0000	0.0718	0.3562
2.0074	0.1150	0.1321	0.5741
3.1913	0.2829	0.1832	0.6824
4.3352	0.4157	0.2304	0.7449
5.4386	0.5132	0.2758	0.7853
6.5127	0.5854	0.3201	0.8135
7.5662	0.6400	0.3639	0.8344
8.6052	0.6825	0.4072	0.8505
9.6336	0.7163	0.4502	0.8634
10.6539	0.7438	0.4931	0.8739
11.6678	0.7665		

2.3.3. Boundary Conditions and Loading Steps

The load was applied in a few steps so that the part had real manufacturing behavior. It was necessary to initially protect the cables of the active reinforcement and later carry out the transfer of efforts to the concrete. During the "initial step", tension was applied to the prestressing strands, since the precast elements are prestressed before concreting. The used command "preset field" applies initial stress to the element. After the first step, "step 1" was started, where the structure received its own weight load (i.e., gravity acting on the structure), which used the properties specified for the material densities. In addition to this loading, the "Tie" command applied between the strands and the concrete started to operate and started the transfer of stresses from the cables to the concrete, in a similar way to the prestressing release in the hollow core slab tracks. Then, "step 2" started. After all the initial stresses, the model came into balance and was ready to receive the displacement (simulating force) application.

2.4. Normative Formulations

2.4.1. NBR 14861 [8]

NBR 14861 [8] demonstrates two ways of verifying the shear strength for prestressed hollow core slabs. The former is performed at the most critical part of the cross-section. The second is expressed in Equations (2) and (3), where they are satisfied for hollow core slabs with no cover and no socket filling.

$$V_{Sd} \leq V_{Rd1} \tag{2}$$

$$V_{Sd} \leq V_{Rd2} \tag{3}$$

where V_{Sd} requesting shear force in the section; V_{Rd1} calculating resistant shear force in the section; and V_{Rd2} the calculating resistant shear force of the compressed diagonals.

The values for the following resistances are obtained using Equations (4) and (5) to calculate the resistant shear force in the section and the calculating resistant shear force of the compressed diagonals, respectively.

$$V_{Rd2} = 0.5 \cdot \nu \cdot f_{cd} \cdot 0.9 \cdot d \cdot \sum b_{w,1} \tag{4}$$

$$V_{Rd1} = \left[0.25 \cdot f_{ctd} \cdot k \cdot (1.2 + 40 \cdot \rho_1) + 0.15 \cdot \sigma_{cp,1}\right] \cdot b_{w,1} \cdot d \tag{5}$$

where f_{cd} is the concrete resistance in compression; d the cross-section height; $\sum b_{w,1}$ width sum; f_{ctd} tensile strength of concrete; ρ_1 reinforcement ratio; $\sigma_{cp,1}$ compressive stress of concrete due to prestressing force; and k is calculated as $1.6 - d \geq 1$ and ν as $0.7 - f_{ck}/200 \geq 0.50$.

When necessary, the resistance to shear stress in hollow core slabs can be increased with the specification of structural cover and/or filling of hollow core. The Brazilian technical standard does not present calculation procedures for hollow core slabs prestressed with openings. For this reason, Pinheiro [20] proposed an adaptation for the calculation, using the sum of the rib widths in the critical section ($\sum b_{w,1}$), equal to the reduced number of ribs. In this paper, the use of structural capping and filling of the hollow core was not addressed, in addition to the use of the adaptation proposed by Pinheiro [20] for calculating the shear force in hollow core slabs with openings.

2.4.2. Eurocode 2 [14]

To calculate the resistant shear force, according to Eurocode, Equation (6) should be used. However, if the value is smaller than that obtained by Equation (7), the second value should be adopted.

$$V_{Rd,c} = \left[C_{Rd,c} \cdot k \cdot (100 \cdot \rho_1 \cdot f_{ck})^{\frac{1}{3}} + k \cdot \sigma_{cp}\right] \cdot b_w \cdot d \tag{6}$$

$$V_{Rd,c} = \left(\nu_{\min} + k \cdot \sigma_{cp}\right) \cdot b_w \cdot d \tag{7}$$

$$k = 1 + \sqrt{\frac{200}{d}} \leq 2 \tag{8}$$

where $V_{Rd,c}$ is the resistant shear force; k is a constant, calculated according to Equation (8) with d in millimeters; d the cross-section height; ρ_1 reinforcement ratio; b_w is the smallest width of the cross-section in the tensile area; and $\sigma_{cp,1}$ compressive stress of concrete due to prestressing force.

2.4.3. ACI 318 [5]

Finally, ACI formulation determines the resistant shear force in three equations, of which the lowest must be used.

$$V_c = \left(0.6 \cdot \lambda \cdot \sqrt{f'_c} + 700 \cdot \frac{V_u \cdot d_p}{M_u}\right) \cdot b_w \cdot d \tag{9}$$

$$V_c = \left(0.6 \cdot \lambda \cdot \sqrt{f'_c} + 700\right) \cdot b_w \cdot d \tag{10}$$

$$V_c = 5 \cdot \lambda \cdot \sqrt{f'_c} \cdot b_w \cdot d \tag{11}$$

where V_c is the resistant shear force; f'_c the compressive strength of concrete; d_p the distance from extreme compression fiber to centroid of prestressed reinforcement; V_u and M_u the factored shear force and moment at section, respectively; b_w is the web width; d the distance from extreme compression fiber to centroid of longitudinal reinforcement; and λ the modification factor to reflect the reduced mechanical properties of lightweight concrete relative to normal weight concrete of the same compressive strength.

3. Results and Discussion

3.1. Experimental Test

Table 5 shows the specimens' geometry collected in this research.

Table 5. Specimen cross-section and material details.

Specimen	Height (mm)	Width (mm)	L (mm)	$\sum bw$ (mm)	Opening
Slab1	206	1234	5982	324	-
Slab2	202	1236	5978	262	Central
Slab3	203	1236	5971	265	Central
Slab4	204	1231	5984	196	Side
Slab5	203	1231	5988	205	Side

Figure 6 shows the specimen after failure for Slab1 (no opening).

(**a**) (**b**)

Figure 6. Slab1 specimen after test: right side view (**a**) and crack pattern under the slab (**b**).

According to the test of Slab1, both sides have shown a typical cracking pattern for shear failure.

Figure 7 shows the specimen after failure for Slab2 (central opening).

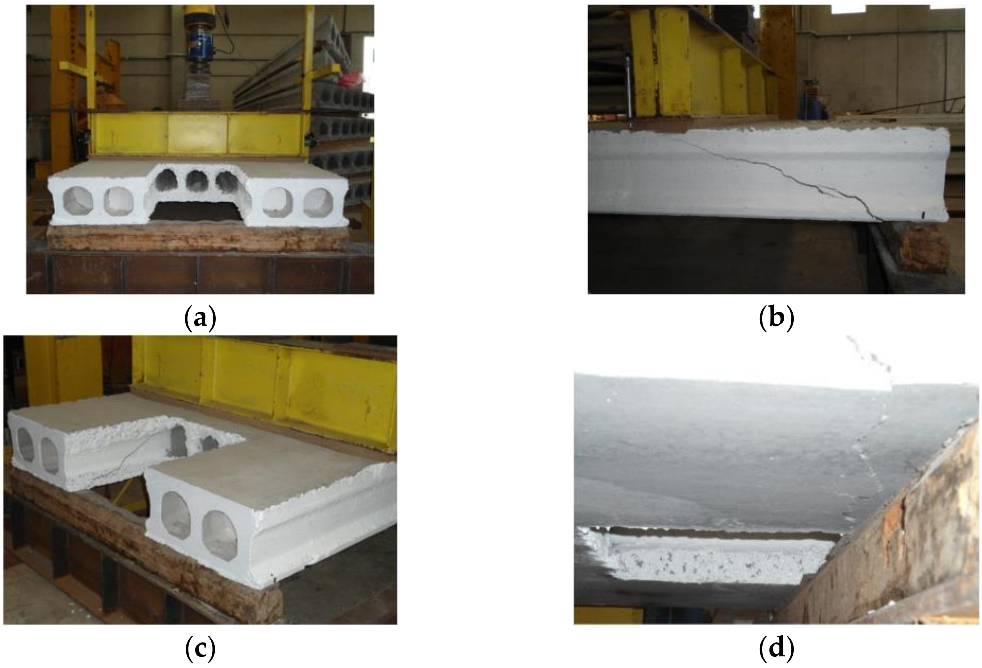

Figure 7. Slab2 specimen: front view (**a**), left side view (**b**), right side view (**c**) and crack pattern under the slab (**d**).

According to the test of Slab2 in Figure 7, the crack patterns shown are typical of shear failure for the left side only. There are no visible signs of cracking on the right side.

Figure 8 shows the specimen when prepared, during test, and after failure for Slab3.

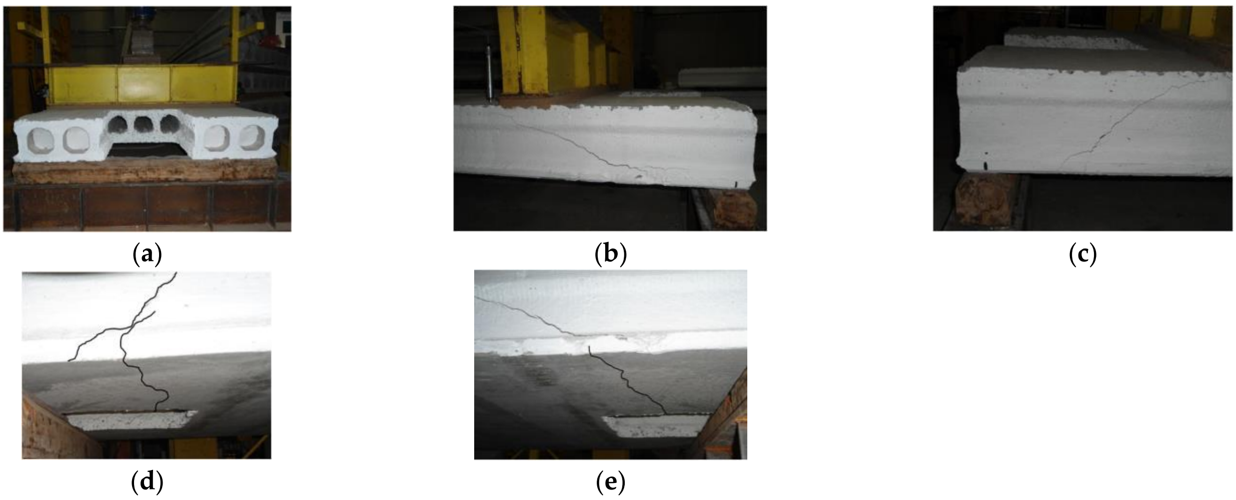

Figure 8. Slab3 specimen: front view (**a**), left side view (**b**), right side view (**c**), crack pattern under the slab (**d**) and bottom view (**e**).

According to the test of Slab3 in Figure 8, the crack patterns shown are typical of shear failure for the left side and bending with shear failure interaction for the right side. In this case, on each side, the crack pattern was different. On the right side, the cracks are mainly caused by rupture by shear force. On the left side, the cracks occurred by shear force with interaction with bending and strand slip.

Figure 9 shows the specimen prepared, during test and after failure for Slab4.

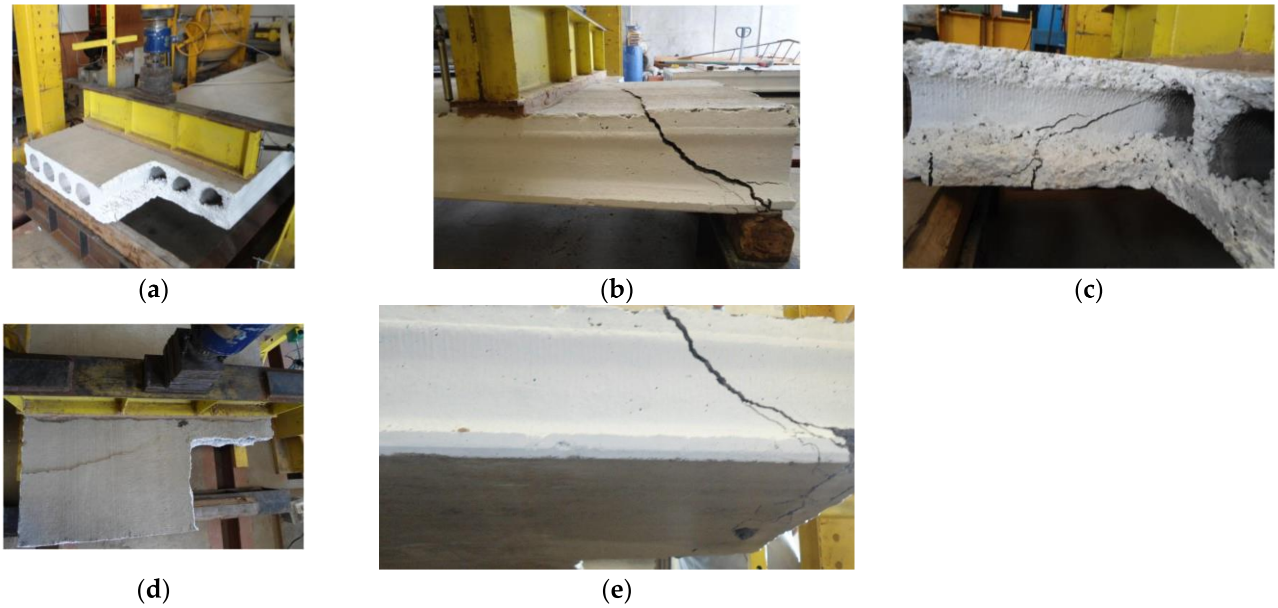

Figure 9. Slab4 specimen: front view (**a**), left side view (**b**), right side view (**c**), crack pattern above the slab (**d**) and under the slab (**e**).

According to the test of Slab4, the crack patterns shown are typical of shear failure for both sides. On the part above the slab, there was a tendency of torsional failure from the right side (opening side), according to Figure 9d,e.

Figure 10 shows the specimen prepared, during test and after failure for Slab5.

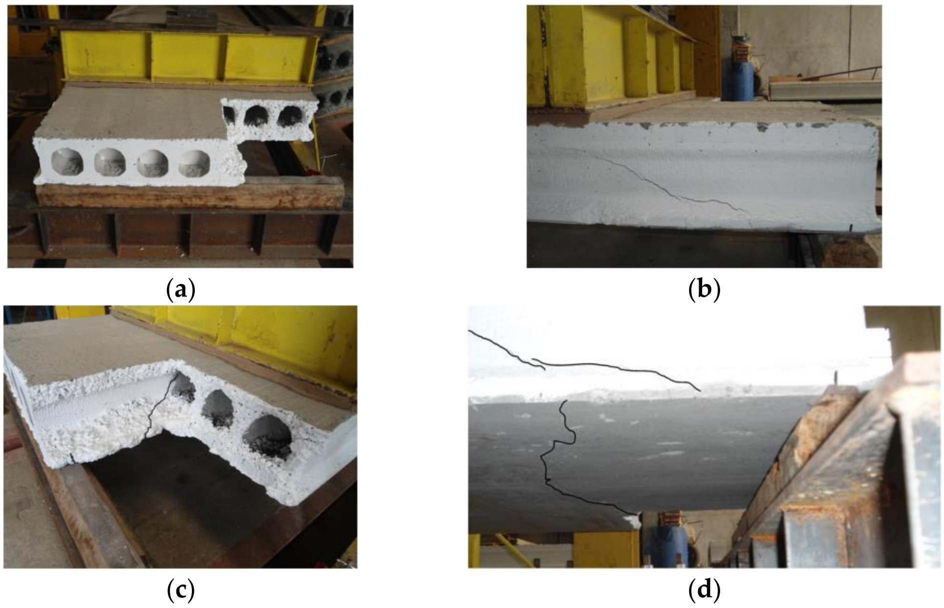

Figure 10. Slab5 specimen: front view (**a**), left side view (**b**), right side view (**c**) and crack pattern under the slab (**d**).

According to the test of Slab5 in Figure 10, the crack patterns shown are typical of shear failure for both sides. On the right side, the cracks are mainly caused by shear force failure. On the left side, the cracks occurred by shear force with interaction with bending and string slip. A torsional tendency could also be observed on the right side of the slab (opening side).

Figure 11 presents the load × displacement curve for the five tested slabs.

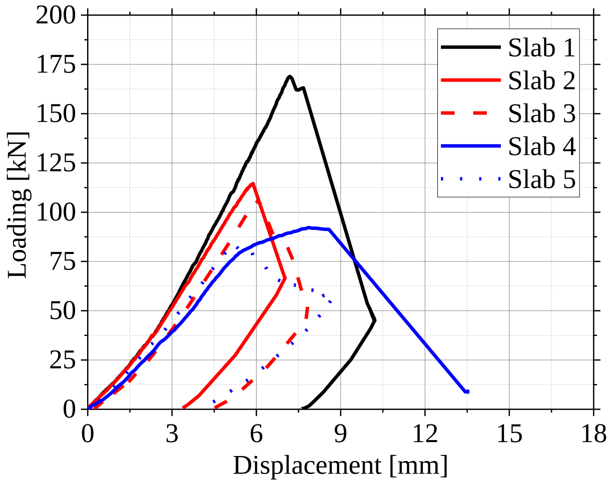

Figure 11. Load × displacement behavior of all performed tests.

Observing the values on five slabs tested, the different values for the same slabs (i.e., the results for slabs 2 and 4 would have to be the same results as for slabs 3 and 5, respectively) may be caused by the accommodation of supports or the unbalance caused by the opening, compromising the local rigidity. Also, considering the difference between the initial sliding strands and the tension on the strands, these can be the causes of the difference between the displacements. Observing Figure 11, Slab2, Slab3 and Slab5 behavior demonstrate a clear shear failure. Slab4 shows a tendency of combined failure of shear and bending, causing torsion along the member.

Table 6 presents the values of strand slip on the slabs before (Ai) and after (Af) the tests.

Table 6. Experimental slip values for slab strands.

Slab		**Strand**							
		I	**II**	**III**	**IV**	**V**	**VI**	**VII**	**VIII**
1	Ai	0.53	0.40	0.77	0.67	0.73	0.42	0.62	0.87
	Af	3.48	3.18	2.97	2.94	2.75	2.45	2.66	3.17
2	Ai	0.47	0.42	0.81	-	-	0.27	0.62	0.96
	Af	2.92	1.74	2.26	-	-	1.18	1.82	1.87
3	Ai	0.40	0.50	0.21	-	-	0.51	0.15	0.68
	Af	2.42	2.51	2.50	-	-	0.51	0.15	0.68
4	Ai	0.68	0.25	1.61	0.96	0.19	-	-	-
	Af	6.44	6.79	6.99	6.60	6.19	-	-	-
5	Ai	0.99	0.92	0.34	1.12	0.93	-	-	-
	Af	2.17	1.42	2.42	2.31	1.69	-	-	-

Following the disposed on Brazilian Standard ABNT NBR 14861 [8], the referred standard establishes the mean value and the maximum value of strand slip, with values shown in Table 7.

Table 7. Mean and maximum values of strand slipping.

Strand Slipping [mm]	**ϕ (mm)**	**l_{pt2} (mm)**	**Aϕ (mm^2)**	**σ_{cp0} (MPa)**	**E (GPa)**
	9.50	**807.50**	**55.69**	**1620**	**199.35**
Δ_{l0}			2.63		
Δ_{llim}			3.42		

According to the values presented in Table 7, the values of the final strand slipping were higher than the maximum value established by the Brazilian standard [8]. It may happen due to the slab-cutting process and the difference in strand stress during manufacturing process, in which strand prestress is performed individually for each strand. Observing the literature, there is no research considering openings on prestressed hollow core slabs submitted to the shear strength test suggested by FIP [13], highlighting the originality of the present research. In the literature, there is research analyzing shear strength using bending tests and different opening locations [1–3], being difficult to compare with the present research.

3.2. Numerical Results

3.2.1. Model Calibration

Initially, the sensitivity study for the models' mesh was carried out. It was observed that the 20 mm mesh showed the best breaking force result, providing a difference of 0.11% between the last value of the 40 mm mesh (Figure 12). Despite requiring a higher computational cost, it was decided to use the 20 mm mesh, as it presents a behavior that is closer to the experimental one.

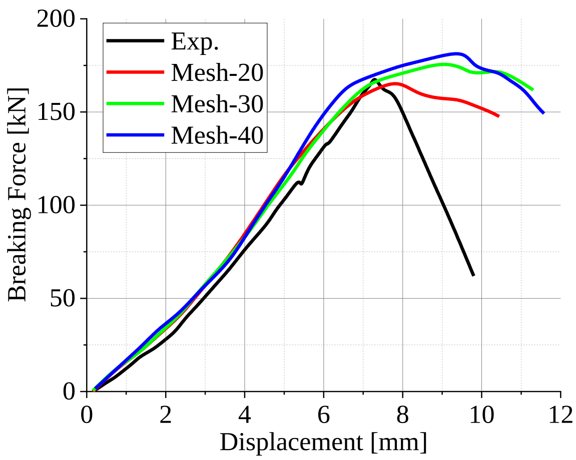

Figure 12. Variation in mesh sizing.

As Nguyen, Tan and Kanda [21] realized, the CDP model presented equation factors that generated great differences in the results. In view of this, it was necessary to calibrate the viscosity parameter (υ) and the expansion angle (ψ). It was observed that for viscosity the best value is 0.0005 (Figure 13a) and for angle (Figure 13b), a value of 28°.

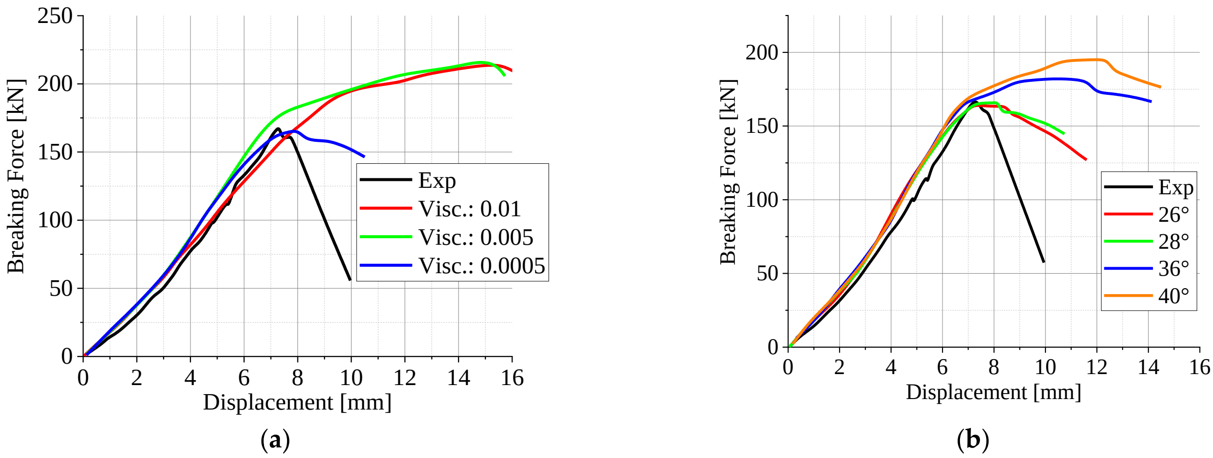

Figure 13. Variation in the viscosity parameter (**a**) and expansion angle (**b**).

3.2.2. Comparison with Experimental Tests

The models' comparison was initially based on the force × displacement curve (Figure 14), between the experimental (Exp.) test and numerical (Num.) results.

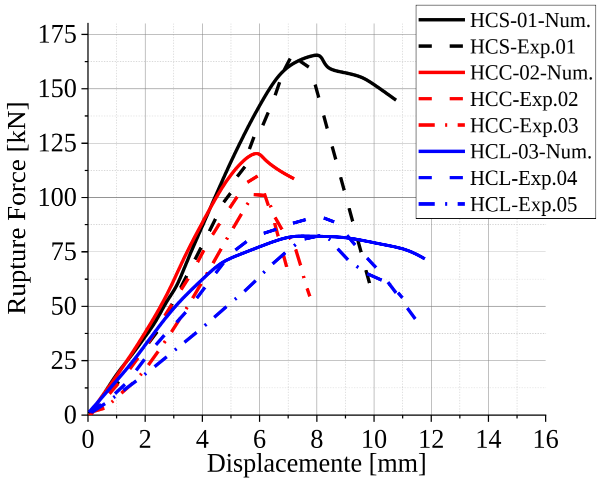

Figure 14. Comparison between force and displacement for all models analyzed.

The model can predict the structural behavior of the hollow core slab HCS-01 for the shear test, showing good agreement with the experimental model performed. The HCC-02 model presented a slight difference in stiffness in relation to the experimental models, However, it remained close to the last forces and displacements. It was noted that the model HCL-03 represented the hollow core slab structural behavior for rupture force testing, due to the closeness of the numerical model curve to the experimental one. Despite the slight difference in stiffness, the model still was able to present forces and displacements equal to the experimental test 05. The difference between the experimental values 04 and 05 occurred due to the production process, test position and other imperfections that can occur in the laboratory.

Therefore, it was observed that the value of ultimate force (*fu*) for the reference model HCS-01 diverged by 1% in relation to the experimental test, just as the model HCL-03 diverged by 0.80%. Both models showed a small difference and very close rupture force values. However, the HCC-02 model was the one that presented a significant divergence of rupture force with 6%, in addition to presenting the most rigid behavior during the test processing. This behavior occurred due to the numerical model boundary conditions. In the experimental test, the slab with the central opening possibly lost more support and contact area. In contrast, the contact used in the numerical simulation remained proportionally distributed in the support region.

Furthermore, the maximum displacements were compared. For the models HCC-02 and HCL-03, the values did not show significant divergence, with differences below 2% of maximum displacement. The HCS-01 model showed greater toughness and, therefore, greater displacement, exceeding by 0.81 mm the hollow core slab of the experimental test. Hence, it is evident that the numerical model was able to move more to the breaking strength, showing a divergence of 11% from the experimental model.

In addition to the force × deformation curves, the cracking pattern was used as a comparison criterion at the point of rupture of each hollow core slab. Captured by the finite element method through tensile damage inserted in the CDP model, Figure 15 shows the tensile damage and the plastic deformation of the concrete for the HCS-01 model.

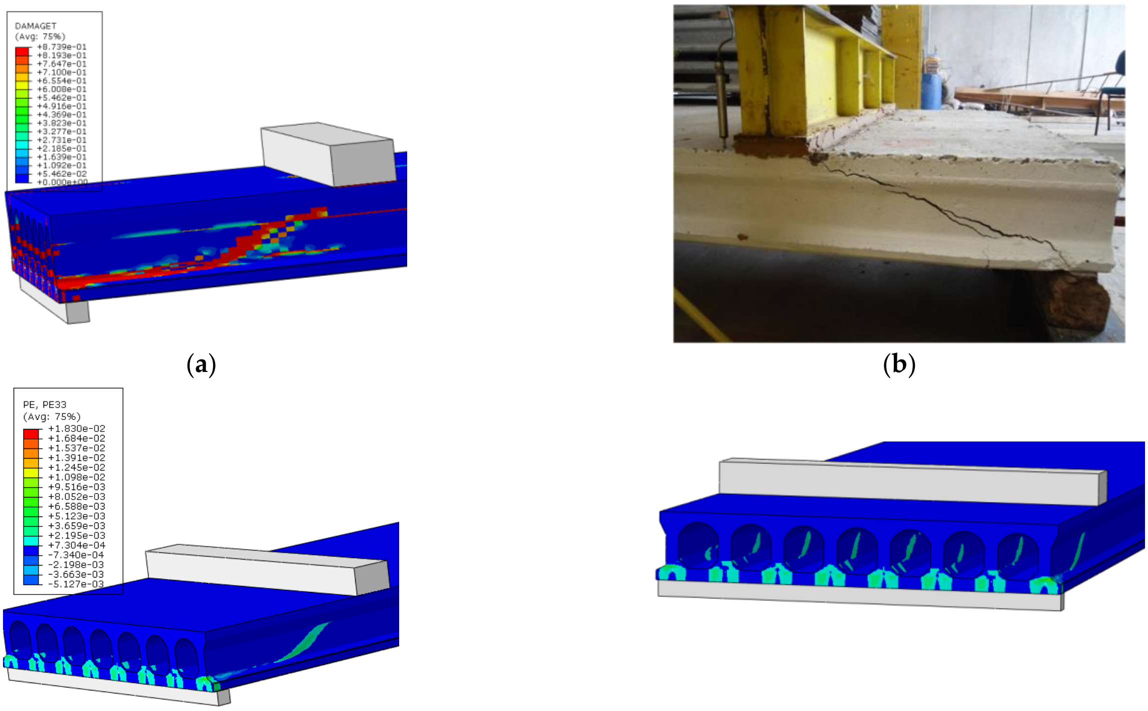

(**a**) (**b**)

(**c**) (**d**)

Figure 15. Numerical analysis of Slab5 specimen: front view (**a**), left side view (**b**), right side view (**c**) and crack pattern under the slab (**d**).

As was observed, the HCS-01 model damage to the traction corresponded to the hollow core slab crack pattern tested in the laboratory. According to the ABAQUS® manual, the tensile damage represents the part in which the material has reached the limit of plasticity. Therefore, there is a consideration of reducing the stiffness in that element. It is still possible to see the plasticized concrete part in the honeycomb slab ribs, with the tensile damage positioning and cracks on a very similar full scale. It was soon noticed that the model broke by cutting force and presented the same pattern as the experimental one.

The tensile damage and the concrete plastic deformation for the HCS-02 model are shown in Figure 16.

It was noticed that the model HCC-02, with a central opening, presented a rupture that is typically due to shear force. The tensile damage obtained was similar to the experimental result, with the inclined crack appearance as demonstrated by Fusco [25]. Furthermore, the opening presence showed greater plastic deformations in the existing ribs, due to the effort's redistribution.

It is shown in Figure 17 that the tensile damage and the concrete plastic deformation for the HCS-03 model.

As can be seen, the rupture mode of the HCL-03 model presented great proximity to the experimental test, typically by shear force. However, as Pinheiro [20] pointed out, in the upper part of the slab there was an apparent tendency to rupture by torsion starting on the right side. Furthermore, it confirmed with the concrete plastic deformation indicated that there were significant deformations in the region.

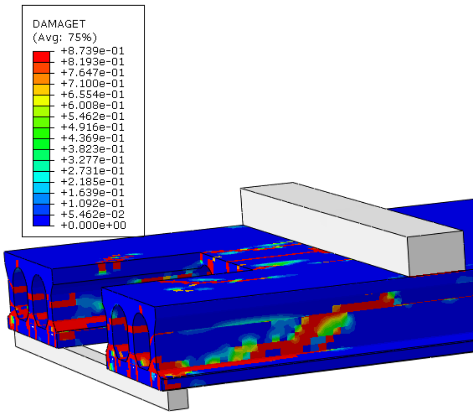

(**a**)

(**b**)

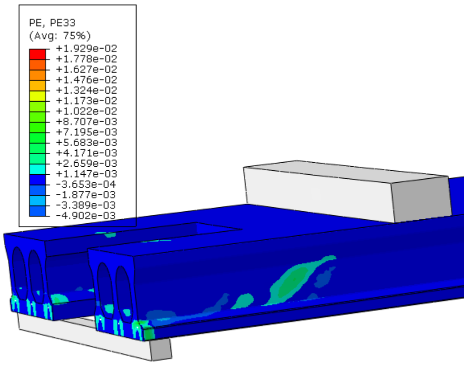

(**c**)

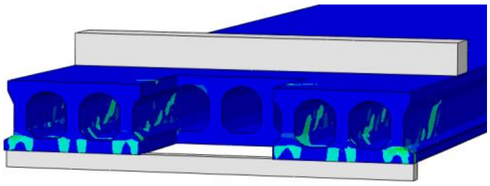

(**d**)

Figure 16. Tensile damage (**a**,**b**) and plastic deformation (**c**,**d**) for HCS-02.

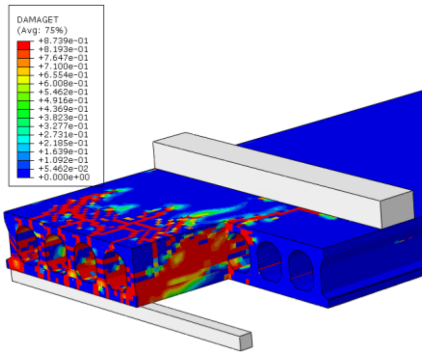

(**a**)

(**b**)

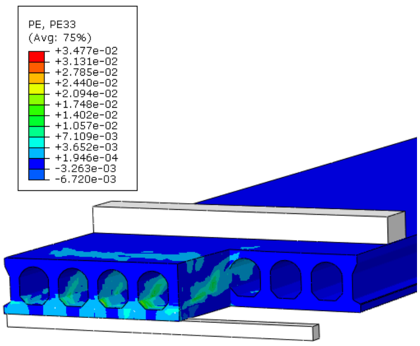

(**c**)

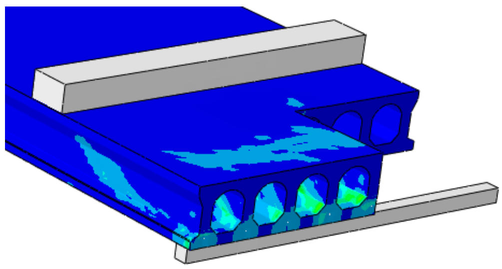

(**d**)

Figure 17. Tensile damage (**a**,**b**) and plastic deformation (**c**,**d**) for HCS-03.

3.3. Normative Results

Once the numerical models' last values were obtained, it was interesting to find out if they were within the normative safety standards. For that, comparisons were made between the experimental results (Vexp) with numerical (Vmef) and formulations (NBR 14861 [8]—V_{NBR}, Eurocode 2 [14]—V_{EUR}, and ACI 318 [5]—V_{ACI}) results. All values are shown in Table 8.

Table 8. Slipping values for slab strands: Comparison of numerical and experimental results.

Shear Force	Models		
	HCS-01	**HCC-02**	**HCL-03**
V_{exp}	164.95 kN	111.98 kN	90.43 kN
V_{mef}	138.56 kN	118.97 kN	85.06 kN
V_{mef}/V_{exp}	0.840	1.062	0.941
V_{NBR}	137.87 kN	111.49 kN	85.10 kN
V_{NBR}/V_{exp}	0.835	0.996	0.941
V_{EUR}	145.71 kN	113.22 kN	86.43 kN
V_{EUR}/V_{exp}	0.883	1.011	0.956
V_{ACI}	177.25 kN	143.33 kN	109.41 kN
V_{ACI}/V_{exp}	1.075	1.280	1.210

As can be seen, the ACI standard was the standard that best predicts the shear strength of hollow core slabs without opening (HCS-01), with an error of only 7.50%. The NBR and Eurocode standards, on the other hand, predict with an error of 16.5% and 11.7%, respectively. The numerical simulation had an error of 16%, very close to the Brazilian standard. Analyzing the slabs with an opening (HCC-02 and HCL-03), the NBR and Eurocode standards were the ones that best predicted the resistant shear force, since the ACI standard has an error of up to 28%. Finally, it is possible to note that the numerical simulation achieved great accuracy in the three slabs' behavior, with errors ranging from 6% to 16%, values very close to the Brazilian standard [8].

4. Conclusions

After this study, the model's result of hollow core slabs with and without openings were obtained, and among these, it is worth mentioning:

i. The values of ultimate strength among the numerical models showed good agreement, diverging by up to 6% from the experimental values, and thus confirmed the functioning of the proposed methodology;

ii. The unopened model typically broke due to shear, according to the diagonal tension, and it was possible to observe the plastic deformation of the concrete along the ribs, with critical cracks appearing as the tensile stress increased;

iii. The model with the central opening showed a redistribution of stresses due to the opening, and thus the most requested ribs were those adjacent to the opening, with the element breaking in this critical section by diagonal traction (break at angle α) and still presenting a decrease in the ultimate strength by 27.25% if compared to the model without opening;

iv. The model with the side opening showed a resistive capacity 50.22% lower than the model without an opening, in addition to presenting high stresses in all ribs above 31.75% and still expressing lower values of shear force. Also, it was observed that the failure mode of this element occurred by diagonal traction (break at angle α); however, there were high deformations in the upper region of the model, with deformations and cracks related to torsional efforts; and

v. It was possible to observe that the presented methodology demonstrated satisfactory results, being able to predict the behavior and the final loads of the prestressed hollow core slab models without openings. It is worth noting that the numerical model presented better results even when compared with the current standards, with the Brazilian standard [8] presenting the best results when compared with ACI [5] and Eurocode [14].

Author Contributions: Conceptualization, A.M.J., A.S. and A.L.C.; methodology, F.A.F.; software, F.N.A.; validation, I.S., V.A. and A.S.; formal analysis, G.P.; investigation, M.F.; resources, H.S.; data curation, A.L.C.; writing—original draft preparation, G.P.; writing—review and editing, F.N.A. and A.S.; visualization, R.C.; supervision, R.C.; project administration, F.A.F.; funding acquisition, H.S. All authors have read and agreed to the published version of the manuscript.

Funding: This research was funded by: CAPES (Coordenação de Aperfeiçoamento de Pessoal de Nível Superior–Finance Code 001), CNPq (Conselho Nacional de Desenvolvimento Científico e Tecnológico) and by the Pró-Reitoria de Pesquisa, Inovação e Pós-Graduação of Instituto Federal de Rondônia (PROPESP/IFRO).

Data Availability Statement: The data presented in this study are available on request from the corresponding author.

Acknowledgments: We would like to acknowledge the Pró-Reitoria de Pesquisa, Inovação e Pós-Graduação of Instituto Federal de Rondônia (PROPESP/IFRO) and the Coordenação de Aperfeiçoamento de Pessoal de Nível Superior-Brazil (CAPES).

Conflicts of Interest: The authors declare no conflict of interest.

References

1. Pachalla, S.K.S.; Prakash, S.S. Load Resistance and Failure Modes of Hollow-Core Slabs with Openings: A Finite Element Analysis. *PCI J.* **2018**, *63*, 25–40. [CrossRef]
2. Mahmoud, K.; Foubert, S.; El-Salakawy, E. Strengthening of prestressed concrete hollow-core slab openings using near-surface-mounted carbonfiber-reinforced polymer reinforcement. *PCI J.* **2017**, *62*, 45–57. [CrossRef]
3. Johnson, T.; Ghadiali, Z. Load distribution test on precast hollow core slabs with openings. *PCI J.* **1972**, *17*, 9–19. [CrossRef]
4. Pachalla, S.K.S.; Prakash, S.S. Load resistance and failure modes of GFRP composite strengthened hollow core slabs with openings. *Mater. Struct.* **2017**, *50*, 1–14. [CrossRef]
5. *ACI 318-19*; Building Code Requirements for Structural Concrete and Commentary. American Concrete Institute: Farmington Hills, MI, USA, 2019. [CrossRef]
6. *EN 1992-1-2*; Eurocode 2: Design of Concrete Structures—Part 1-2: General Rules—Structural Fire Design. European Committee for Standardization (CEN): Brussels, Belgium, 2008.
7. *ABNT NBR 6118*; Design of Concrete Structures—Procedure. Brazilian National Standards Organization: Rio de Janeiro, Brazil, 2014. (In Portuguese)
8. *ABNT NBR 14861*; Pre-Molded Prestressed Hollow Core Slabs—Requirements and Procedures. Brazilian National Standards Organization: Rio de Janeiro, Brazil, 2011. (In Portuguese)
9. Pachalla, S.K.S.; Prakash, S.S. Efficient near surface mounting CFRP strengthening of pretensioned hollowcore slabs with opening—An experimental study. *Compos. Struct.* **2017**, *162*, 28–38. [CrossRef]
10. Yang, L. Design of prestressed hollow core slabs with reference to web shear failure. *J. Struct. Eng.* **1994**, *120*, 2675–2696. [CrossRef]
11. Araujo, C.A.M.; Loriggio, D.D.; Da Camara, J.M.M.N. Anchorage failure and shear design of hollow-core slabs. *Struct. Concr.* **2011**, *12*, 109–119. [CrossRef]
12. Confort, A.; Ortiz-Navas, F.; Piemont, A.; Plizzari, G.A. Enhancing the shear strength of hollow-core slabs by using polypropylene fibres. *Eng. Struct.* **2020**, *207*, 110172. [CrossRef]
13. FIP. *Quality Assurance of Hollow Core Slab Floors*; SETO: Lausanne, Switzerland, 1992.
14. *EN 1992-1-1*; Eurocode 2: Design of Concrete Structures—Part 1-1: General Rules and Rules for Buildings. European Committee for Standardization (CEN): Brussels, Belgium, 2011.
15. *ABNT NBR 16697*; Portland Cement—Requirements. Brazilian National Standards Organization: Rio de Janeiro, Brazil, 2018. (In Portuguese)
16. *ABNT NBR 5738*; Concrete—Procedure for Molding and Curing Specimens. Brazilian National Standards Organization: Rio de Janeiro, Brazil, 2016. (In Portuguese)
17. *ABNT NBR 5739*; Concrete—Cylindrical Specimen Compression Test. Brazilian National Standards Organization: Rio de Janeiro, Brazil, 2018. (In Portuguese)
18. ArcelorMittal. *Wires and Strands for Prestressed Concrete*; ArcelorMittal: Luxembourg, 2015. (In Portuguese)
19. *EN 1168*; Precast Concrete Products—Hollow Core Slabs. European Committee for Standardization (CEN): Brussels, Belgium, 2011.

20. Pinheiro, G.L. Study on the Influence of Openings and Oblique Cuts in the Resistance to Shear Stress in Prefabricated Prestressed Hollow Core Slabs. Ph.D. Thesis, Graduate Program in Structures and Civil Construction, Federal University of São Carlos, São Carlos, Brazil, 2017; 269p. (In Portuguese).
21. Nguyen, T.N.H.; Tan, K.; Kanda, T. Invesigations on web-shear behavior of deep precast, prestressed concrete hollow core slabs. *Eng. Struct.* **2019**, *183*, 579–593. [CrossRef]
22. Lubliner, J.; Oliver, J.; Oller, S.; Oñate, E. Plastic-damage model for concrete. *Int. J. Solids Struct.* **1989**, *25*, 299–326. [CrossRef]
23. Lee, J.; Fenves, G.L. Plastic-damage model for cyclic loading of concrete structures. *J. Eng. Mech.* **1998**, *124*, 892–900. [CrossRef]
24. Guo, Z. *Principles of Reinforced Concrete*; Elsevier: Oxford, UK, 2014.
25. Fusco, P.B. *Concrete Structures—Tangential Stresses*, 1st ed.; Pini: São Paulo, Brazil, 2008. (In Portuguese)